Updated Measurement of the CP-Violating Phase $\phi_s^{J/\psi\phi}$ Using Flavor-tagged Decay $B_s^0 \to J/\psi\phi$

(Dated: July 22, 2010)

We report an updated measurement of the CP-violating phase $\phi_s^{J/\psi\phi}$ and the decay width difference for the two mass eigenstates $\Delta\Gamma_s$ from flavor-tagged decay $B_s^0 \to J/\psi\phi$: $\Delta\Gamma_s = 0.15 \pm 0.06\,(\text{stat}) \pm 0.01\,(\text{syst})$ ps^{-1}, $\phi_s^{J/\psi\phi} = -0.76^{+0.38}_{-0.36}\,(\text{stat}) \pm 0.02\,(\text{syst})$. The allowed 95% C.L. intervals are $0.014 < \Delta\Gamma_s < 0.263$ ps^{-1}, $-1.65 < \phi_s^{J/\psi\phi} < 0.24$ and $-0.235 < \Delta\Gamma_s < -0.040$ ps^{-1}, $1.14 < \phi_s^{J/\psi\phi} < 2.93$. The data sample corresponds to an integrated luminosity of 6.1 fb^{-1} accumulated with the D0 detector at the Fermilab Tevatron collider.

Preliminary Results for Summer 2010 Conferences

I. INTRODUCTION

In the standard model (SM), the light (L) and heavy (H) mass eigenstates of the mixed B_s^0 system are expected to have sizeable mass and decay width differences: $\Delta M_s \equiv M_H - M_L$ and $\Delta\Gamma_s \equiv \Gamma_L - \Gamma_H$. The two mass eigenstates are expected to be almost pure CP eigenstates. The CP-violating phase that appears in $b \to c\overline{c}s$ decays, due to the interference of the decay with and without mixing, is predicted [1, 2] to be $\phi_s^{J/\psi\phi} = -2\beta_s = 2\arg[-V_{tb}V_{ts}^*/V_{cb}V_{cs}^*] = -0.038 \pm 0.002$, where V_{ij} are elements of the Cabibbo-Kobayashi-Maskawa quark-mixing matrix [3]. New phenomena may alter the observed phase [4–14] to $\phi_s^{J/\psi\phi} \equiv -2\beta_s + \phi_s^{\Delta}$.

The analysis of the decay chain $B_s^0 \to J/\psi\phi$, $J/\psi \to \mu^+\mu^-$, $\phi \to K^+K^-$ separates the CP even and CP odd states using the angular distributions of the decay products as a function of proper time. The first direct constraint on $\phi_s^{J/\psi\phi}$[15] was derived analysing $B_s^0 \to J/\psi\phi$ decays where the flavor (B_s^0 or $\overline{B_s^0}$) at the time of production was not tagged. It was followed by an improved analysis, PRL08 [16], that included the information on the B_s^0 flavor at time zero, and was based on a larger data set. Here we present new D0 results, based on an even larger data sample, reconstructed and selected with an improved algorithm. We measure $\Delta\Gamma_s$, the average lifetime of the B_s^0 system, $\overline{\tau}_s = 1/\overline{\Gamma}_s$, where $\overline{\Gamma}_s \equiv (\Gamma_H + \Gamma_L)/2$, and the CP-violating phase $\phi_s^{J/\psi\phi}$. The data sample corresponds to an integrated luminosity of 6.1 fb^{-1} collected with the D0 detector [17] at the Fermilab Tevatron collider.

II. DATA SELECTION AND RECONSTRUCTION

The work presented here is based on data accumulated by the D0 detector [17] between February 2002 and June 2009. The event selection follows that in Refs. [15, 16]. Events are required to include two reconstructed muons of opposite charge, detected in the muon chambers inside the toroid magnet. At least one of the muons is also required to be detected in the muon chambers outside the toroid magnet. These muons are used to reconstruct J/ψ candidates in the invariant mass range 2.9 – 3.3 GeV. These J/ψ candidates are then combined with another pair of oppositely charged tracks, consistent with the decay $\phi \to K^+K^-$. The ϕ candidate was required to have an invariant mass between 1.00 – 1.03 GeV to form B_s^0 candidates. In the kinematic fit under the B_s^0 decay hypothesis, we constrain the dimuon invariant mass to the world-average value of the J/ψ mass and we constrain the four-track system to a common vertex. We set the minimum values of momenta in the transverse plane for B_s^0, ϕ, and K meson candidates at 6.0 GeV, 1.5 GeV, and 0.7 GeV, respectively. To ensure a good measurement of the proper decay length and of track momenta we require each track to have at least two SMT hits, and least a total of eight SMT and CFT hits, and the uncertainty of the proper decay length to be below 60 μm. Successful B_s^0 candidates are required to have an invariant mass in the range 5.0 – 5.8 GeV. All multiple J/ψ or ϕ candidates make multiple B_s^0 candidates in a given event, we select the one B_s^0 with the better vertex fit probability.

To reconstruct the primary vertex, we select tracks that are not used as decay products of the B_s^0 candidate. We apply a constraint to the average beam-spot position. In the presence of multiple $p\overline{p}$ interactions, the B_s^0 candidate may be associated with the wrong interaction vertex. We eliminate such occurrences by requiring that the distance along the beam direction between the primary and decay vertices be less than 5 cm. While this effect was negligible in the early data, it happens on average in about 1% of currently collected events due to the gradually increasing average instantaneous luminosity.

We define the signed decay length of a B_s^0 meson L_{xy}^B as the vector pointing from the primary vertex to the decay vertex, projected on to the B_s^0 transverse momentum. The proper decay length of a B_s^0 candidate is given by

$$ct = \frac{M_{B_s}\vec{L}_{xy} \cdot \vec{p}}{p_T^2},$$

where M_{B_s} is the world-average B_s^0 mass. The invariant mass distribution of the accepted 82809 candidates is shown in Fig. 1. The curves are projections of the maximum likelihood fit, described in Section IV.

III. FLAVOR TAGGING

The flavor of the initial state of the B_s^0 candidate is determined by exploiting properties of particles produced by the other B hadron ("opposite-side tagging", or OST). Work is in progress on tuning the independent flavor-tagging algorithm utilizing the information on the tracks accompanying the B_s^0 meson decay products ("same-side" tagging) for the increasingly busy environment due to the increasing instantaneous luminosity. The same-side tagging is not used for the earlier data for consistency across the whole sample.

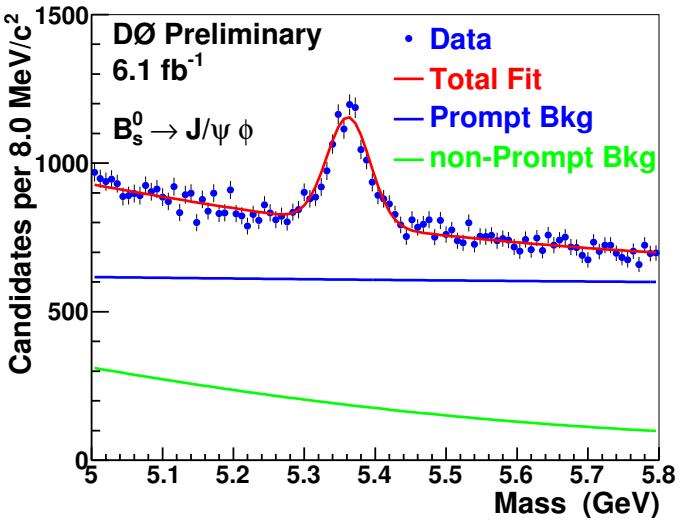

FIG. 1: The invariant mass distribution of the $(J/\psi, \phi)$ system for B_s^0 candidates. The curves are the projections of the maximum likelihood fit: prompt and non-prompt background and total (see Section IV).

The OST discriminators are based primarily on the presence of a muon or an electron from the decay of the other B hadron produced in the $p\overline{p}$ interaction. If a charged lepton is not found, the algorithm attempts to reconstruct the decay vertex of the opposite-side B hadron and determine the net charge of tracks forming the vertex.

The following OST discriminating variables are used in the present analysis:

- Muon jet charge, $muonJet$
- Secondary vertex (SV) charge (if muon and SV identified), $muonSVCharge$
- Electron jet charge: $electronJet$
- Secondary vertex charge (if electron and SV identified), $electronSVCharge$
- Secondary vertex charge, $svCharge$
- Event charge (all opposite-side tracks), $eventCharge$

The algorithm, based on the Likelihood Ratio method, assigns to each event a value of the predicted discriminator variable d, in the range [−1,1], with $d > 0$ for the initial b quark, combining the above information as follows: If a muon candidate is found, $muonJet$ and $muonSVCharge$ variables are used. If no muon is present, but an electron is found, we use $electronJet$ and $electronSVCharge$. If no muons or electrons are found, but there is an SV, we use $svCharge$ and $eventCharge$. In any other case the discriminating variable is set to 0. The algorithm and the OST discriminating variables are described in detail in Ref. [19].

The predicted discriminating variable d is calibrated with data for which the flavor (B or $\overline{B}$) is known. The tagging dilution $\mathcal{D}$ is defined as:

$$\mathcal{D} = \frac{N_{\rm cor} - N_{\rm wr}}{N_{\rm cor} + N_{\rm wr}} \tag{1}$$

where $N_{\rm cor}$ ($N_{\rm wr}$) is the number of events with correctly (wrongly) identified initial B_s^0 meson flavor.

The current dilution calibration is based on three independent real data samples:

- $B \to \mu\nu D^{*\pm}$ (Run IIA, as used in Ref.[19]),
- $B^{\pm} \to J/\psi K^{\pm}$ (Run IIA)
- $B^{\pm} \to J/\psi K^{\pm}$ (Run IIB)

$\lvert d\rvert$	$J/\psi K$(IIA)	$J/\psi K$(IIB)	μD^*(II)	$\lvert\mathcal{D}\rvert$ weighted mean
$0.00-0.10$	14.05 ± 8.51	-0.17 ± 7.22	–	5.78 ± 5.51
$0.10-0.20$	23.38 ± 9.25	19.06 ± 6.89	8.4 ± 3.1	11.32 ± 2.70
$0.20-0.35$	14.38 ± 7.56	21.59 ± 6.19	23.6 ± 2.7	22.42 ± 2.35
$0.35-0.45$	37.60 ± 7.76	38.60 ± 8.89	38.5 ± 3.4	38.38 ± 2.94
$0.45-0.60$	58.23 ± 8.39	52.37 ± 7.27	51.2 ± 3.2	52.13 ± 2.77
$0.60-1.00$	90.37 ± 29.43	48.75 ± 13.30	59.7 ± 5.8	58.97 ± 5.23

TABLE I: Opposite-side tagging (OST) dilution values (in %) extracted from self-tagging real data samples for different ranges of the discriminator variable $|d|$.

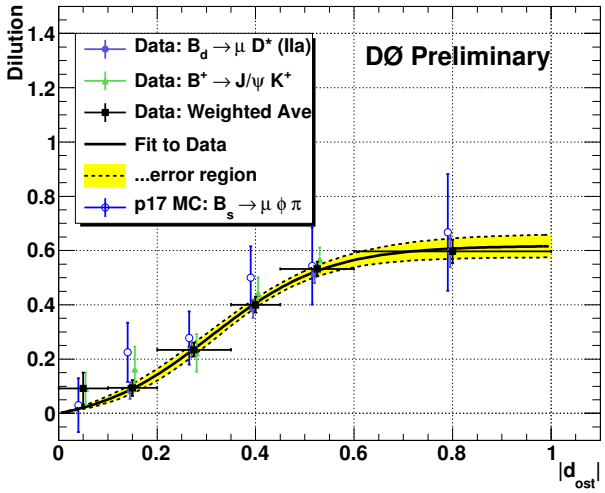

FIG. 2: Resulting parametrization of the dilution $|\mathcal{D}|$ as a function of the discriminator variable $|d|$ for the combined opposite-side tagger. The curve is the result of the weighted fit to three self tagging real data samples (see text). Comparisons to a MC simulation are also shown.

The run dependence (we refer to the first running period corresponding to 1.3 fb^{-1} as Run IIA) of the $B \to \mu\nu D^{*\pm}$ data was checked by performing an analysis of the $B^0_d - \overline{B^0_d}$ oscillation [20] for the Run IIB subsample. The amplitude was found to be very close to unity, confirming the stability of the flavor-tagging performance. The measured values of the dilution for the three data samples above, in different ranges of $|d|$, are summarized in Table I and shown in Fig. 2. All three measurements are in good agreement and hence a weighted average is taken.

The dependence of the dilution on the discriminator variable $|d|$ is parametrized as

$$|\mathcal{D}| = p_0/(1+\exp((p_1-|d|)//p_2)) - p_0/(1+\exp(p_1/p_2)). \quad (2)$$

The efficiency ϵ of the OST described here is 18%.

IV. MAXIMUM LIKELIHOOD FIT

IV-A. Likelihood function

We perform an unbinned maximum likelihood fit to the proper decay time, three decay angles characterizing the final state, and the mass of the B^0_s candidate. The likelihood function $\mathcal{L}$ is given by:

$$\mathcal{L} = \prod_{i=1}^{N} [f_{\rm sig}\mathcal{F}^i_{\rm sig} + (1-f_{\rm sig})\mathcal{F}^i_{\rm bck}], \quad (3)$$

where N is the total number of events, and $f_{\rm sig}$ is the fraction of signal in the sample. The function $\mathcal{F}^i_{\rm sig}$ describes the distribution of the signal in mass, proper decay time, decay angles, and flavor tagging probability. For the signal mass distribution, we use a Gaussian function with free mean and width. The proper decay time distribution of the L or H component of the signal is parametrized by an exponential convoluted with a Gaussian function. The width of the Gaussian is taken from the event-by-event estimate of the ct uncertainty $\sigma(ct)$, scaled by an overall calibration factor, s, determined from the fit to the prompt component of the background. $\mathcal{F}^i_{\rm bck}$ is a sum of two components.

"Prompt" background is due to directly produced J/ψ mesons accompanied by random tracks arising from hadronization. This background is distinguished from "non-prompt" background (see section IV IV-D), where the J/ψ meson is a product of a B-hadron decay while the tracks forming the ϕ candidate emanate from a multibody decay of a B hadron or from hadronization. Each component of $\mathcal{F}^i_{\rm bck}$ is a product of the corresponding mass, proper decay time and angular function. The signal and background parametrization is described below. There are 33 free parameters in the fit.

IV-B. Signal time-dependent angular distribution

We assume that the (K^+K^-) system in the decay $B^0_s \to J/\psi K^+K^-$ is in a P-wave. Our studies of the decay $B^0_s \to J/\psi K^+K^-$ indicate that the data are consistent with no (K^+K^-) S-wave component (see Appendix A), and we do not include it in our fit. In a similar analysis, the CDF Collaboration included an S-wave component and found a negligible [27] fraction consistent with zero. The decay amplitude of the B^0_s and $\overline{B}^0_s$ mesons is decomposed into three independent components corresponding to linear polarization states of the vector mesons J/ψ and ϕ, which are either longitudinal (0) or transverse to their direction of motion, and parallel ($\|$) or perpendicular ($\perp$) to each other. The time evolution of the angular distribution of the decay products, expressed in terms of the magnitudes $|A_0|$, $|A_\|$, and $|A_\perp|$, and two relative strong phases $\delta_1 = -\delta_{||} + \delta_\perp$ and $\delta_2 = -\delta_0 + \delta_\perp$ of the amplitudes, is given in Refs. [25, 26]:

$$
\begin{aligned}
&\frac{d^4\Gamma}{dtd(\cos\theta)d\varphi d(\cos\psi)} \propto \\
&\quad 2\cos^2\psi(1-\sin^2\theta\cos^2\varphi)|A_0(t)|^2 \\
&\quad +\sin^2\psi(1-\sin^2\theta\sin^2\varphi)|A_\|(t)|^2 \\
&\quad +\sin^2\psi\sin^2\theta|A_\perp(t)|^2 \\
&\quad +(1/\sqrt{2})\sin 2\psi\sin^2\theta\sin 2\varphi{\rm Re}(A^*_0(t)A_\|(t)) \\
&\quad +\ (1/\sqrt{2})\sin 2\psi\sin 2\theta\cos\varphi{\rm Im}(A^*_0(t)A_\perp(t)) \\
&\quad -\ \sin^2\psi\sin 2\theta\sin\varphi{\rm Im}(A^*_\|(t)A_\perp(t)).
\end{aligned}
\tag{4}
$$

Polarization amplitudes for B^0_s (upper sign) and $\overline{B}^0_s$ (lower sign) are given by the following equations:

$$
\begin{aligned}
|A_{0,\|}(t)|^2 &= |A_{0,\|}(0)|^2\left[\mathcal{T}_+ \pm e^{-\overline{\Gamma}t}S\ \sin(\Delta M_s t)\right], \\
|A_\perp(t)|^2 &= |A_\perp(0)|^2\left[\mathcal{T}_- \mp e^{-\overline{\Gamma}t}S\ \sin(\Delta M_s t)\right],
\end{aligned}
$$

$$
\begin{aligned}
{\rm Re}(A^*_0(t)A_\|(t)) &= |A_0(0)||A_\|(0)|\cos(\delta_2-\delta_1) \\
&\times\left[\mathcal{T}_+ \pm e^{-\overline{\Gamma}t}S\ \sin(\Delta M_s t)\right],
\end{aligned}
$$

$$
\begin{aligned}
{\rm Im}(A^*_0(t)A_\perp(t)) &= |A_0(0)||A_\perp(0)|| \\
&\times[e^{-\overline{\Gamma}t}(\ \pm\sin\delta_2\cos(\Delta M_s t)\ \mp\cos\delta_2\sin(\Delta M_s t)C) - \\
&(1/2)(e^{-\Gamma_H t}-e^{-\Gamma_L t})S\ \cos\delta_2],
\end{aligned}
$$

$$
\begin{aligned}
{\rm Im}(A^*_\|(t)A_\perp(t)) &= |A_\|(0)||A_\perp(0)| \\
&\times[\ e^{-\overline{\Gamma}t}(\ \pm\sin\delta_1\cos(\Delta M_s t)\mp\cos\delta_1\sin(\Delta M_s t)C) \\
&-(1/2)(e^{-\Gamma_H t}-e^{-\Gamma_L t})S\ \cos\delta_1],
\end{aligned}
$$

where $\mathcal{T}_\pm = (1/2)\left[(1 \pm C)e^{-\Gamma_L t} + (1 \mp C)e^{-\Gamma_H t}\right]$, $S = \sin(\phi_s^{J/\psi\phi})$, and $C = \cos(\phi_s^{J/\psi\phi})$. In the coordinate system of the J/ψ rest frame (where the ϕ meson moves in the x direction, the z axis is perpendicular to the decay plane of $\phi \to K^+K^-$, and $p_y(K^+) \geq 0$), the transversity polar and azimuthal angles (θ, φ) describe the direction of the μ^+, and ψ is the angle between $\vec{p}(K^+)$ and $-\vec{p}(J/\psi)$ in the ϕ rest frame.

For a given event, the decay rate is the sum of the B_s^0 and $\overline{B}_s^0$ rates weighted by probability $\mathrm{P}(B_s) = (1-\mathcal{D})/2$ and $\mathrm{P}(\overline{B}_s) = 1 - \mathrm{P}(B_s)$, respectively. It is multiplied by the detector acceptance factor that is a product of the acceptance factors in the three angles. All events, independent of the tagging information are used in the fit. Events that lack a flavor tag, i.e. that have $\mathcal{D} = 0$, still contribute to the measurement of $\phi_s^{J/\psi\phi}$ through the $\cos(\phi_s^{J/\psi\phi})$ dependence of $\mathcal{T}_\pm$ and through the term proportional to $(e^{-\Gamma_H t} - e^{-\Gamma_L t})S$.

IV-C. Signal acceptance correction

Following the procedure of PRL08, we model the acceptance of the three angles (θ, φ, ψ) by fits using polynomial functions, with parameters determined using MC simulations. Events generated uniformly in the three-angle space are processed through the standard GEANT-based [28] simulation of the D0 detector, and reconstructed and selected as real data. Simulated events are weighted to match the kinematic distributions observed in the data. The details of the weighting procedure and acceptance measurement for this sample are given in Appendix B.

IV-D. Background model

The proper decay time distribution of the background is described as a sum of a prompt component, modeled as a Gaussian function centered at zero, and a non-prompt component. The non-prompt component is modeled as a superposition of one exponential for $t < 0$ and two exponentials for $t > 0$, with free slopes and normalizations. The distribution of the background in mass is described by a linear and a quadratic function for the prompt and non-prompt component, respectively. For the angular distributions we use the functions: $(1 + X_2 \cos^2\theta + X_4 \cos^4\theta)$, $(1 + Y_1 \cos(2\varphi) + Y_2 \cos^2(2\varphi))$, and $(1 + Z_2 \cos^2\psi)$. For each of the above background functions we use two separate sets of free parameters for the prompt and non-prompt components.

V. FIT RESULTS

In Ref. [16] we reported a $\phi_s^{J/\psi\phi}$ measurement based on a subset of the present data, corresponding to an integrated luminosity of 2.8 fb^{-1}. In that analysis, we applied a loose constraint to the strong phases δ_i in order to remove an ambiguity in the results for $\phi_s^{J/\psi\phi}$ and $\Delta\Gamma_s$. We also fixed the value of ΔM_s to the mean value of the CDF result [29]. Later, when averaging the D0 and CDF measurements [30], we removed the δ_i constraint, and replaced the fixed value of ΔM_s by a Gaussian constraint. In this analysis, we explore fits with and without δ_i constraints, and apply a Gaussian constraint of $\Delta M_s = 17.77 \pm 0.12$ ps^{-1}. Ensemble tests, presented in Appendix C, verify the fit results for all physics quantities for the case of the constrained strong phases. For free δ_i, we find a non-negligible bias. The peak of the distribution $\phi_s^{J/\psi\phi}$ is moved towards a higher absolute value by about 15% of the input value, while the peak in the fitted $\Delta\Gamma_s$ distribution is shifted up by 0.03 ps^{-1}. Thus, we present the point estimates, along with the C.L. intervals, for the scenario with constrained strong phases only. For the free δ_i case, the proper estimate of the bias as a function of parameter values requires more studies.

The decay $B_s^0 \to J/\psi\phi$ is related to $B_d^0 \to J/\psi K^*$ by the U(3) flavor symmetry. Gronau and Rosner [31] discuss the similarity between the two processes and argue that the magnitudes of the polarization amplitudes should be similar and their phases should agree within 0.17 radians. The complex amplitudes for the $B_d^0 \to J/\psi K^*$ decay have been measured with small uncertainties [32]. We have performed a fit, applying a constraint to the values of Ref. [32]: $\delta_1 = -0.42 \pm 0.18$ and $\delta_2 = 3.01 \pm 0.14$. Fit results are presented in Table II. For the polarization amplitudes, we obtain $A_\perp(0) = 0.44 \pm 0.03$, and $|A_0(0)|^2 - |A_{||}(0)|^2 = 0.35 \pm 0.03$, in agreement with the B_d^0 world-average values of 0.469 ± 0.013 and 0.363 ± 0.005, respectively. This agreement between the magnitude of amplitudes for the B_s^0 and B_d^0 decays provides an empirical justification for applying constraints to their relative phases. Also shown are results for the two subsamples, corresponding to the first 2.8 fb^{-1} and the last 3.3 fb^{-1} of exposure. The likelihood profile as a function of $\phi_s^{J/\psi\phi}$ is shown in Fig. 3. The likelihood profile as a function of $\Delta\Gamma_s$ is shown in Fig. 4. Fit projections on the B_s^0 candidate proper decay length, and the three decay angles are shown in Figs. 5 and 6.

	Full Sample	First 2.8 fb^{-1}	Last 3.3 fb^{-1}
All Candidates	82808	47442	35366
Signal	3435 ± 84	1999 ± 66	1449 ± 50
B_s^0 Mass (MeV)	5362.4 ± 0.8	5362.2 ± 1.0	5362.7 ± 1.2
B_s^0 Mass Width (MeV)	30.4 ± 0.7	29.5 ± 0.9	31.7 ± 1.1
Proper length error scale	1.268 ± 0.006	1.261 ± 0.007	1.271 ± 0.008
$\overline{\tau}_s$ (ps)	1.47 ± 0.04	1.45 ± 0.07	1.46 ± 0.06
$\Delta\Gamma_s$ (ps^{-1})	0.15 ± 0.06	0.23 ± 0.08	0.07 ± 0.07
$A_\perp(0)$	0.44 ± 0.03	0.42 ± 0.04	0.47 ± 0.04
$\lvert A_0(0)\rvert^2 - \lvert A_\parallel(0)\rvert^2$	0.35 ± 0.03	0.32 ± 0.04	0.40 ± 0.04
$\phi_s^{J/\psi\phi}$	-0.76 ± 0.37	-0.86 ± 0.33	-0.37 ± 0.81

TABLE II: Summary of results of the maximum likelihood fit for the case with strong phases constrained to the world-average values for the $B_d^0 \to J/\psi K^*$ decay. The second and third columns show results for two subsamples of comparable exposure. Only the solution with $\Delta\Gamma_s > 0$ is shown. All uncertainties shown here are parabolic, symmetric one-standard deviation estimates from MINUIT.

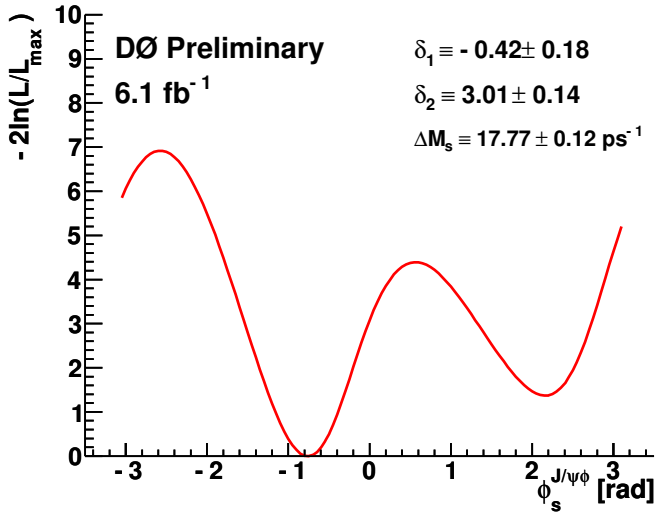

FIG. 3: The likelihood variation as a function of $\phi_s^{J/\psi\phi}$ for the fit with strong phases constrained to the world-average values for the $B_d^0 \to J/\psi K^*$ decay [32].

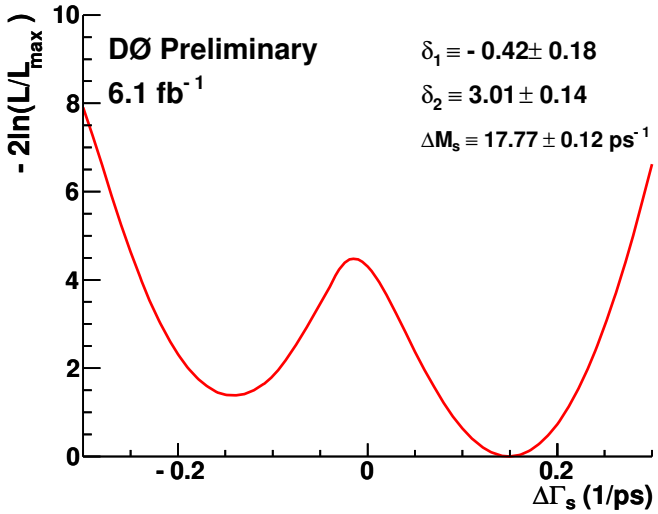

FIG. 4: The likelihood variation as a function of $\Delta\Gamma_s$ for the fit with strong phases constrained to the world-average value for the $B_d^0 \to J/\psi K^*$ decay [32].

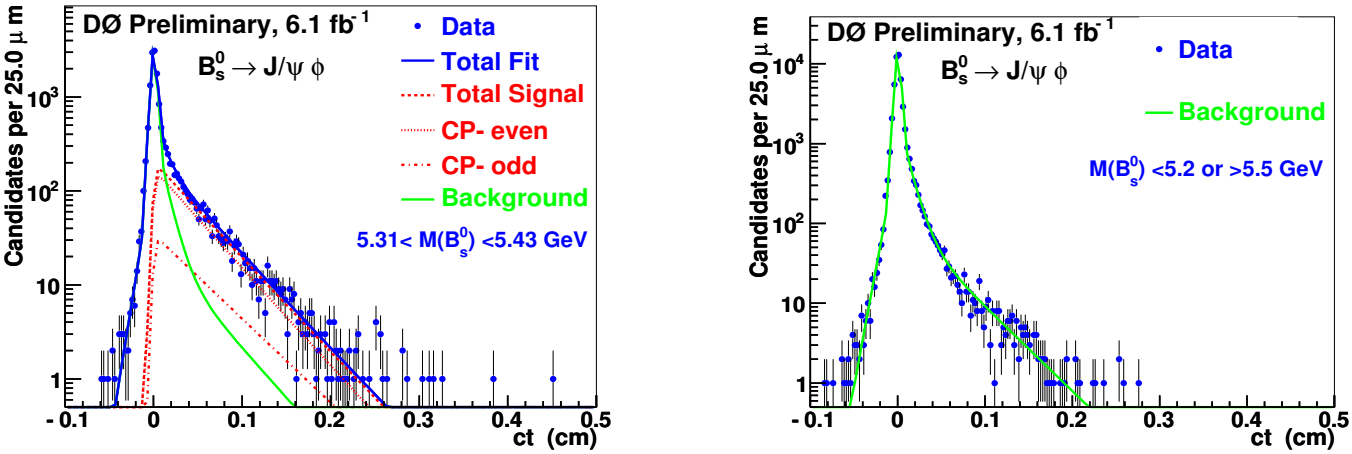

FIG. 5: The proper decay length distribution for B_s^0 candidates in the indicated signal mass range (left) and in the indicated background mass range (right) The curves are the projections of the maximum likelihood fit.

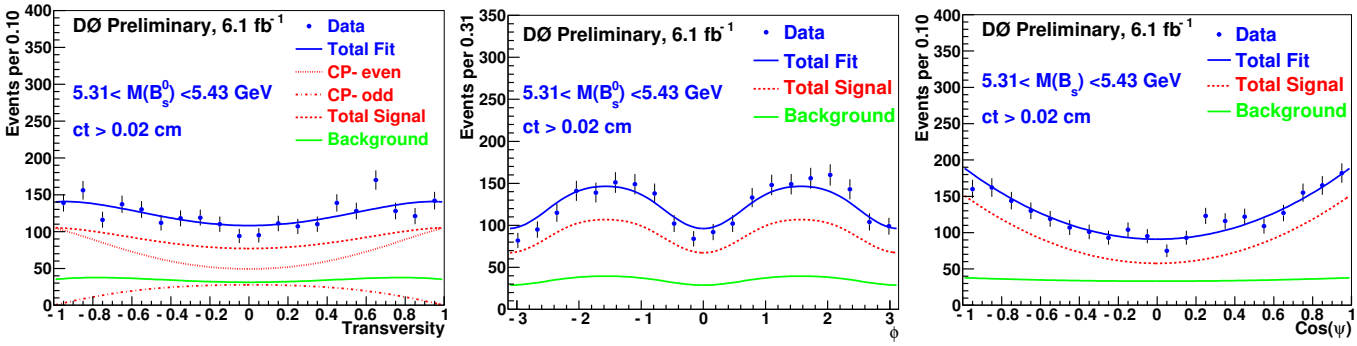

FIG. 6: The transversity polar angle $\cos(\theta)$ (left), the transversity azimuthal angle φ (center), and $\cos(\psi)$ (right) distributions in the indicated signal region. The curves are the projections of the maximum likelihood fit. The $\cos(\psi)$ distribution shows no sign of forward-backward asymmetry that would be indicative of KK S-wave.

VI. CONFIDENCE REGION AND SYSTEMATIC UNCERTAINTIES

As done previously [36], to obtain the C.L. contours in the $\phi_s^{J/\psi\phi}$ - $\Delta\Gamma_s$ plane that account for non-Gaussian behavior of the likelihood, we adjust the two-dimensional likelihood profiles by applying a likelihood - C.L. conversion curve determined in an ensemble study to ensure correct statistical coverage. Details of the study are presented in Appendix C.

Many systematic uncertainties are included in the fit by treating them as nuisance parameters, for example, placing a Gaussian constraint equivalent to the uncertainty on ΔM_s, fitting for the parameterization of backgrounds. There are additional uncertainties due to the limited knowledge of external constants used in the fit. The only such constants are those describing the flavor-tagging calibration and the detector acceptance. To account for the related systematic effects on the confidence region, we generate ensembles for a number of "alternative universes", with external constants varied within their uncertainties. For the flavor tagging dilution, and for the detector acceptance, we vary the coefficients of the parameterization by $\pm$ 1σ. For the MC weighting, we use the difference between the fitted curve and the full histogram.

The effects of varying the external parameters on the measured physics quantities are summarized in Table III.

Source	$\overline{\tau}_s$ ps	$\Delta\Gamma_s$ ps^{-1}	$A_\perp(0)$	$\phi_s^{J/\psi\phi}$
Matching the MC kinematics to data	$\pm$0.001	$\pm$0.001	$\pm$0.001	$\pm$0.01
Acceptance function	$\pm$0.01	$\pm$0.01	$\pm$0.01	$\pm$0.01
Flavor tagging parameters	$\pm$0.001	$\pm$0.001	$\pm$0.001	$\pm$0.01
Total	$\pm$0.01	$\pm$0.01	$\pm$0.01	$\pm$0.02

TABLE III: Estimate of external systematic uncertainties.

We obtain the following results: $\Delta\Gamma_s = 0.15 \pm 0.06\,(\text{stat}) \pm 0.01\,(\text{syst})$ ps^{-1} and $\phi_s^{J/\psi\phi} = -0.76^{+0.38}_{-0.36}\,(\text{stat}) \pm 0.02\,(\text{syst})$. The allowed 95% C.L. intervals are $0.014 < \Delta\Gamma_s < 0.263$ ps^{-1}, $-1.65 < \phi_s^{J/\psi\phi} < 0.24$ and $-0.235 < \Delta\Gamma_s < -0.040$ ps^{-1}, $1.14 < \phi_s^{J/\psi\phi} < 2.93$. The C.L. contours in the $\phi_s^{J/\psi\phi}$ - $\Delta\Gamma_s$ plane, corrected for the C.L. coverage and for major systematic uncertainties, are shown in Fig. 7.

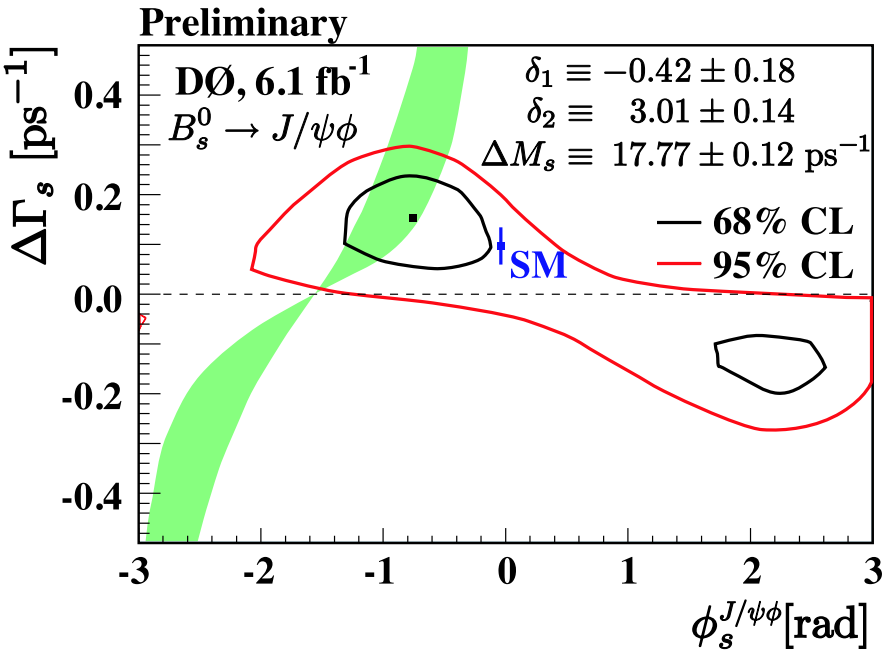

FIG. 7: 68% and 95% C.L. contours in the plane $\Delta\Gamma_s$ - $\phi_s^{J/\psi\phi}$. Also shown is the 68% contour from the D0 dimuon charge asymmetry analysis [37]. The comparison is made under the assumption of a single source of the CP violation in the B_s^0 - $\overline{B}_s^0$ mixing.

VII. DISCUSSION

A question may arise about the statistical uncertainty of the $\phi_s^{J/\psi\phi}$ result, in particular whether it is understood why the present measurement is not more precise than the PRL08 result, and why the last half of the data results in a considerably larger uncertainly.

In this multi-dimensional problem, with strong correlations among measurable (see Table IV), the statistical uncertainty of a given parameter does not necessarily scale with the inverse square-root of the signal size.

	$A_\perp(0)$	$\Delta\Gamma_s$	$\phi_s^{J/\psi\phi}$
$\overline{\tau}_s$	-0.40	-0.03	0.71
$A_\perp(0)$		-0.54	-0.36
$\Delta\Gamma_s$			-0.18

TABLE IV: Correlation coefficients for physics parameters.

The ensemble test (Appendix C) shows the expected range for the statistical error of $\phi_s^{J/\psi\phi}$. The present result is close to the median value of 0.39. For the two subsamples, the uncertainty is below and above the appropriate median, but still in the expected range at that statistics.

The sensitivity to $\phi_s^{J/\psi\phi}$ depends on the value of $\Delta\Gamma_s$: the larger $\Delta\Gamma_s$, the deeper and narrower the likelihood minimum as a function of $\phi_s^{J/\psi\phi}$. Without flavor tagging the dependence of $\phi_s^{J/\psi\phi}$ vanishes for $\Delta\Gamma_s = 0$. This is illustrated in Fig. 8 that shows likelihood scans as functions of $\phi_s^{J/\psi\phi}$ for three discrete values of $\Delta\Gamma_s$. The measured values of $\Delta\Gamma_s$ for the two subsamples, while consistent with each other, are above the overall average for the 2.8 fb^{-1} subsample, and below the average for the 3.3 fb^{-1} subsample, resulting in the $\phi_s^{J/\psi\phi}$ uncertainty being smaller and larger for the two subsamples, respectively, as expected.

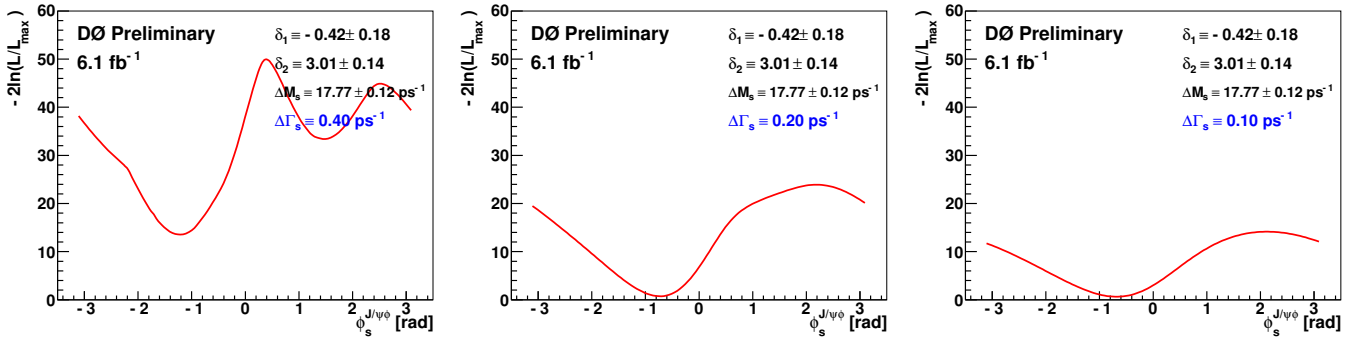

FIG. 8: Likelihood profiles for $\phi_s^{J/\psi\phi}$ at fixed values of $\Delta\Gamma_s$.

Fit to the untagged data

It is a unique feature of the decay $B_s^0 \to J/\psi\phi$ that thanks to the sizeable lifetime difference between the two mass eigenstates, there is a sensitivity to $\phi_s^{J/\psi\phi}$ through the interference terms between the CP-even and CP-odd waves, even when the oscillatory terms proportional to $\sin(\Delta M_s t)$ cancel out. The interference terms $A_\parallel - A_\perp$ and $A_0 - A_\perp$ are proportional to $(e^{-\Gamma_H t} - e^{-\Gamma_L t})\sin\phi_s$ and don't vanish in the absence of the flavor-tagging information. Also, if $\cos(\phi_s)$ is significantly different from unity, the decay rates of the CP-even and CP-odd components have two slopes each. From a fit ignoring the flavor-tagging information, with constrained δ_i, we obtain $\phi_s^{J/\psi\phi} = \pm(0.90 \pm 0.42)$, $\Delta\Gamma_s = 0.15 \pm 0.06$ ps^{-1}, or $\phi_s^{J/\psi\phi} = \pm(2.24 \pm 0.42)$, $\Delta\Gamma_s = -0.15 \pm 0.06$ ps^{-1}.

Comparison with previous D0 results

In Ref. [16] we reported a $\phi_s^{J/\psi\phi}$ measurement based on a subset of the present data, corresponding to an integrated luminosity of 2.8 fb^{-1}. We have repeated the present analysis using only the data from that earlier running period. There are several changes in the present analysis, in addition to the use of opposite-side instead of combined flavor tagging:

- Improvements in the track reconstruction efficiency
- Refinement in the B_s^0 vertex fitting and in the proper time uncertainty calculation
- Detector acceptance corrections derived for the present data set
- Using a constraint to ΔM_s within the experimental uncertainty instead of a fixed value
- Using a Gaussian constraint to the latest world-average values to the strong phases

Results of the present analysis for the PRL08 running period are shown in the second column in Table II. A fit to the same data sample, using the combined flavor tagging, yields $\overline{\tau}_s = 1.47 \pm 0.07$ ps, $\Delta\Gamma_s = 0.23 \pm 0.08$ ps^{-1}, $\phi_s^{J/\psi\phi} = -0.75 \pm 0.32$. We have also performed a fit using the old data sample, exactly as it was selected in the PRL08 analysis, and obtained $\overline{\tau}_s = 1.51 \pm 0.05$ ps, $\Delta\Gamma_s = 0.18 \pm 0.05$ ps^{-1}, $\phi_s^{J/\psi\phi} = -0.62 \pm 0.27$. The published result was $\overline{\tau}_s = 1.52 \pm 0.06$ ps, $\Delta\Gamma_s = 0.19 \pm 0.07\,(\text{stat})\,^{+0.02}_{-0.01}\,(\text{syst})$ ps^{-1}, and the CP-violating phase, $\phi_s^{J/\psi\phi} = -0.57^{+0.24}_{-0.30}\,(\text{stat})\,^{+0.07}_{-0.02}\,(\text{syst})$. We find the present results consistent with the published results.

VIII. ADDITIONAL ANALYSIS CROSS CHECKS

The complete process of event detection, reconstruction and selection, and of the fitting procedure is validated by fitting simulated signal events that have been passed through the full detector simulation and event reconstruction.

To simulate the decay $B_s^0 \to J/\psi\phi$, we use the EvtGen generator [39], interfaced to Pythia [41]. The package EvtGen was developed jointly by the BaBar and CLEO collaborations. The part relevant to this analysis, PVV_CPLH, simulating a decay of a neutral pseudoscalar to a pair of vector states, allowing for CP violation and a lifetime difference between the light and heavy components of the parent doublet, includes modifications by the LHCb collaboration [40], and was further modified and adapted for D0.

We analyze samples of pure B_s^0 and pure $\overline{B}_s^0$, generated with $\overline{\tau}_s = 1.46$ ps, $\Delta\Gamma_s = 0.09$ ps^{-1}, and different values of $\phi_s^{J/\psi\phi}$. The size of each file is approximately three times the size of the signal in the real data.

In the fits, we allow for background that may result from incorrect pattern recognition - if, e.g. one of the kaon tracks is not reconstructed, and a random fragmentation track is used as a ϕ decay product. In the fit, such events contribute to the "non-prompt" background. The fits assign $\approx 85\%$ of events to signal. Table V presents the fit results. For a better estimate of the significance of the deviation of the $\phi_s^J/\psi\phi$ from the input value, we repeat the fits setting $\phi_s^{J/\psi\phi}$ to the input value, and calculate the value of $2\Delta \ln \mathcal{L}$. The results are shown in the last column (for fits with fixed δ_i only). The sum for nine independent measurements is equivalent to the χ^2 and is equal to 9.8, corresponding to a probability of 0.37 and we conclude that no significant bias is observed in the $\phi_s^{J/\psi\phi}$ results.

We find no bias in other fit results. The result for $\overline{\tau}_s$, averaged over fits to all samples is 1.46 ± 0.01 ps, and for $\Delta\Gamma_s$ it is 0.09 ± 0.01 ps^{-1}. For the fits with fixed δ_i the results are 1.46 ± 0.01 ps and 0.09 ± 0.01 ps^{-1}.

State	Input $\phi_s^{J/\psi\phi}$	$\overline{\tau}_s$ (ps)	$\Delta\Gamma_s$ (ps^{-1})	$\phi_s^{J/\psi\phi}$	$2\Delta \ln \mathcal{L}$	s standard deviations
B_s^0	-1.0	1.453 ± 0.029	0.095 ± 0.037	$-2.10^{+0.30}_{-0.26}$	5.2	2.28
$\overline{B}_s^0$	-1.0	1.454 ± 0.023	0.080 ± 0.051	-0.90 ± 0.36	0.05	0.22
B_s^0	1.0	1.400 ± 0.033	0.145 ± 0.057	1.33 ± 0.27	0.61	0.78
$\overline{B}_s^0$	1.0	1.483 ± 0.023	0.074 ± 0.037	1.00 ± 0.36	0.0	0.0
B_s^0	-0.5	1.473 ± 0.015	0.055 ± 0.024	-0.17 ± 0.27	1.42	1.19
$\overline{B}_s^0$	-0.5	1.434 ± 0.022	0.073 ± 0.045	$-0.56^{+0.45}_{-0.53}$	0.01	0.10
B_s^0	0.5	1.480 ± 0.024	0.120 ± 0.032	$0.03^{+0.32}_{-0.30}$	2.38	1.54
$\overline{B}_s^0$	0.5	1.512 ± 0.023	0.101 ± 0.032	0.60 ± 0.28	0.14	0.37
B_s^0	0.0	1.465 ± 0.022	0.109 ± 0.031	-0.19 ± 0.32	0.07	0.26

TABLE V: Summary of results of the maximum likelihood fits to MC samples of pure B_s^0 and pure $\overline{B}_s^0$ events generated with different values of $\phi_s^{J/\psi\phi}$, as indicated at each line. The input values of the mean lifetime and of the decay rate difference are $\overline{\tau}_s = 1.46$ ps and $\Delta\Gamma_s = 0.09$ ps^{-1}. The uncertainties of the measurements are symmetric, parabolic Minuit errors, and hence are underestimated. For a more accurate measure of the significance of the residuals for $\phi_s^{J/\psi\phi}$, we also show the difference in $2 \cdot \ln \mathcal{L}$ between the best fit and the fit with $\phi_s^{J/\psi\phi}$ set to the input value.

IX. CONCLUSIONS

In summary, we have reported an updated measurement of the B_s^0 mixing parameters in the decay process $B_s^0 \to J/\psi\phi$. We assume CP conservation in the B_s^0 decay, but allow for a free mixing-induced $CP-$violating phase. We constrain the oscillation frequency to $\Delta M_s = 17.77 \pm 0.12$ ps^{-1}, as measured in Ref. [29]. From a fit with an additional constraint of the phases of the polarization amplitudes to the world-average values from the decay $B_d^0 \to J/\psi K^*$, [32] we obtain $\Delta\Gamma_s = 0.15 \pm 0.06\,(\text{stat}) \pm 0.01\,(\text{syst})$ ps^{-1}, $\phi_s^{J/\psi\phi} = -0.76^{+0.38}_{-0.36}\,(\text{stat}) \pm 0.02\,(\text{stat})$. The allowed 95% C.L. intervals are $0.014 < \Delta\Gamma_s < 0.263$ ps^{-1}, $-1.65 < \phi_s^{J/\psi\phi} < 0.24$ and $-0.235 < \Delta\Gamma_s < -0.040$ ps^{-1}, $1.14 < \phi_s^{J/\psi\phi} < 2.93$.

[1] A. Lenz, and U. Nierste, J. High Energy Physics **0706**, 072 (2007).
[2] M. Bona *et al.*, J. High Energy Physics **0610**, 081 (2006).
[3] M. Kobayashi and T. Maskawa, Prog. Theor. Phys. **49**, 652 (1973).
[4] A. J. Buras, Nucl. Phys. proc. Supp. **185**, 157 (2008) and references therein.
[5] Z. Ligeti *et al.*, arXiv:1006.0432 hep-ph.
[6] A. J. Buras *et al.*, arXiv:1005.5310 hep-ph.
[7] B. A. Dobrescu, P. J. Fox and A. Martin, arXiv:1005.4238 hep-ph.
[8] J. P. Saha, B. Misra and A. Kundu, arXiv:1003.1384 hep-ph.
[9] A. J. Buras *et al.*, arXiv:1002.2126 hep-ph.
[10] G. Isidori, Y. Nir, G. Perez, arXiv:1002.0900 hep-ph.
[11] A. Soni *et al.*, arXiv:1002.0595 hep-ph.
[12] L L. Everett *et al.*, arXiv:0911.5349 hep-ph.
[13] F. J. Botella, G. C. Branco and M. N.Rebelo, arXiv:0911.1853 hep-ph.
[14] C. W.Chiang *et al.*, JHEP, **1004**, 031, 2010.
[15] D0 Collaboration, V. M. Abazov *et al.*, Phys. Rev. Lett. **98**, 121801 (2007).
[16] D0 Collaboration, V. M. Abazov *et al.*, Phys. Rev. Lett. **101**, 241801 (2008).
[17] D0 Collaboration, V. M. Abazov *et al.*, Nucl. Instrum. Methods Phys. Res. A **565**, 463 (2006).
[18] D0 Collaboration, V. M. Abazov *et al.*, Phys. Rev. D **76**, 057101 (2007).
[19] D0 Collaboration, V. M. Abazov *et al.*, Phys. Rev. D **74**, 112002 (2006).
[20] V. M. Abazov *et al.* [D0 Collaboration], Phys. Rev. Lett. **97**, 021802 (2006) [arXiv:hep-ex/0603029].
[21] OPAL Collaboration, R. Akers *et al.*, Z. Phys. **C 66**, 19 (1995).
[22] G.Borissov, A.Rakitin, Flavor Tagging Technique for B_s Mesons, D0 Note 5210.
[23] http://www-d0.hef.kun.nl//fullAgenda.php?ida=a091637
[24] http://www-d0.fnal.gov/Run2Physics/ckm/d0_private/mixing/dilution.html
[25] A. S. Dighe, I. Dunietz and R. Fleischer, Eur. Phys. J. C **6**, 647 (1999), [arXiv:hep-ph/9804253].
[26] I. Dunietz, R. Fleischer, and U. Nierste, Phys. Rev. D **63**, 114015 (2001).
[27] CDF Collaboration, http://www-cdf.fnal.gov/physics/new/bottom/100513.blessed-BsJpsiPhi_5.2fb/
[28] R. Brun and F. Carminati, CERN Program Library Long Writeup W5013, 1993 (unpublished).
[29] CDF Collaboration, A. Abulencia *et al.*, Phys. Rev. Lett. **97**, 242003 (2006).
[30] http://www.-d0.fnal.gov/Run2Physics/WWW/results/prelim/B/B59/.
[31] M. Gronau, J. L. Rosner, Phys. Lett. B **669**, 321 (2008).
[32] C. Amsler *et al.* (Particle Data Group), PL B667, 1 (2008) and 2009 partial update for the 2010 edition (URL: http://pdg.lbl.gov).
[33] M. Suzuki, Phys. Rev. D **64**, 117503 (2001).
[34] BaBar Collaboration, B. Aubert *et al.*, Phys. Rev. D **71**, 032005 (2005).
[35] CDF Collaboration, A. Abulencia *et al.*, Phys. Rev. Lett. **100**, 161802 (2008).
[36] D0 Collaboration, http://www.-d0.fnal.gov/Run2Physics/WWW/results/prelim/B/B58/.
[37] D0 Collaboration, V. M. Abazov *et al.*, arXiv:1007.0395[hep-ex], accepted for publication in Phys. Rev. D.
[38] H.G. Moser and A. Roussarie, Nucl. Instrum. Methods Phys. Res. Sect. A **384**, 491 (1997).
[39] D.J. Lange, Nucl. Instrum. Meth. A **462**, 152 (2001).
[40] We thank the PVV_CPLH author, T. du Pree, and the LHCb collaboration, for providing us access to the code.
[41] H. U. Bengtsson and T. Sjostrand, Comp. Phys. Comm. **46**, 43 (1987).

APPENDIX A: THE K^+K^- SYSTEM

The decay $B_s^0 \to J/\psi K^+K^-$ is dominated by the quasi-two body process $B_s^0 \to J/\psi\phi$, but it may have a contribution from an S-wave K^+K^- system produced directly or via a decay of the wide state $f_0(980)$. The situation is analogous to that of the B_d^0 decay to charmonium and the $K\pi$ system which has been analysed in detail in Ref. [34]. With the S wave included, the differential decay rate has four additional terms, corresponding to the S-wave quadratic term and the $S-P$ wave interference terms.

The term corresponding to the interference of the S wave with the A_0 amplitude is proportional to $\cos(\psi)$, and does not vanish after integration over the other two angles. Thus, a significant presence of the S wave should manifest itself by a forward-backward asymmetry in $\cos(\psi)$. Such an asymmetry was observed in the $K\pi$ system and an S-wave component was found necessary to describe the data. In this case, the magnitude and sign of the asymmetry was found to be strongly varying with the $K\pi$ mass in the vicinity of the K^* resonance, reflecting the resonant phase motion. The present data do not show such effect. The $\cos(\psi)$ distribution is symmetric around zero, as seen in Fig. 6. To quantify the symmetry and its independence of $M(KK)$, we compare the number of events at $\cos(\psi) < 0$ and $\cos(\psi) > 0$, in five $M(KK)$ mass intervals in the vicinity of the ϕ resonance. The result is shown in Fig. 9. The overall forward-backward asymmetry is -0.02 ± 0.02.

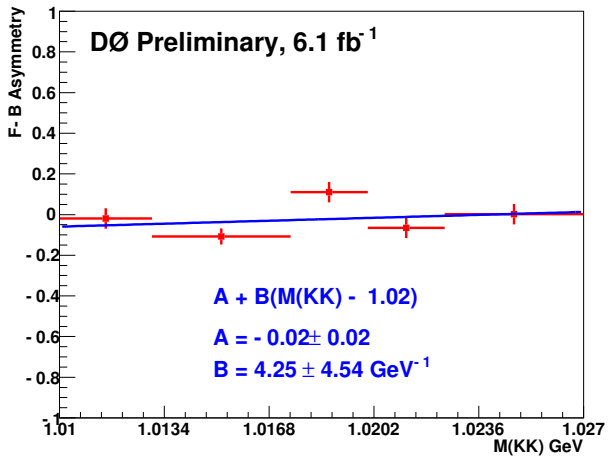

FIG. 9: The forward-backward asymmetry in the distribution of $\cos(\psi)$ in five intervals of $M(KK)$.

APPENDIX B: DETECTOR ACCEPTANCE

We take into account the shaping of the signal distribution by the detector acceptance and kinematic selection by introducing the acceptance functions in the three angles. To obtain the acceptance in each angle, we use the distribution of accepted events for a MC sample generated uniformly in the space of the three relevant angles. Since the p_T distributions of final-state objects in the MC sample may be different from the distributions in data, we introduce a weighting factor as a function of $p_T(J/\psi)$, separately for the central and forward regions. The weight is obtained by dividing the p_T distributions of J/ψ originating from B_s^0 in data and in MC. For data, the histogram is filled with the number of signal events found in each bin.

The behavior of the weight factor as a function of $p_T(J/\psi)$ for the central and forward regions is shown in Fig. 10. The weight can be obtained from the bin contents in Fig. 10, or from a fitted smooth curve. The difference between the two is a measure of the systematic uncertainty due to the modeling of the detector acceptance as a function of final-state momenta. We use the histogram contents as a default, and use the parametrized weight function as an alternative.

The acceptance in all three angles, φ, θ, and ψ is shown in Fig 11. Also shown are fitted curves of the form: $F(\varphi) = 1 + J\cos(2\varphi) + K\cos^2(2\varphi)$, $G(cos\theta) = 1 + B\cos^2\theta + C\cos^4\theta$, and $H(\psi) = 1$. The fitted values of the acceptance parameters are: $B = 0.36 \pm 0.06$, $C = -0.28 \pm 0.07$, $J = -0.057 \pm 0.007$, and $K = -0.059 \pm 0.014$. We find the acceptance to be independent of the angle ψ.

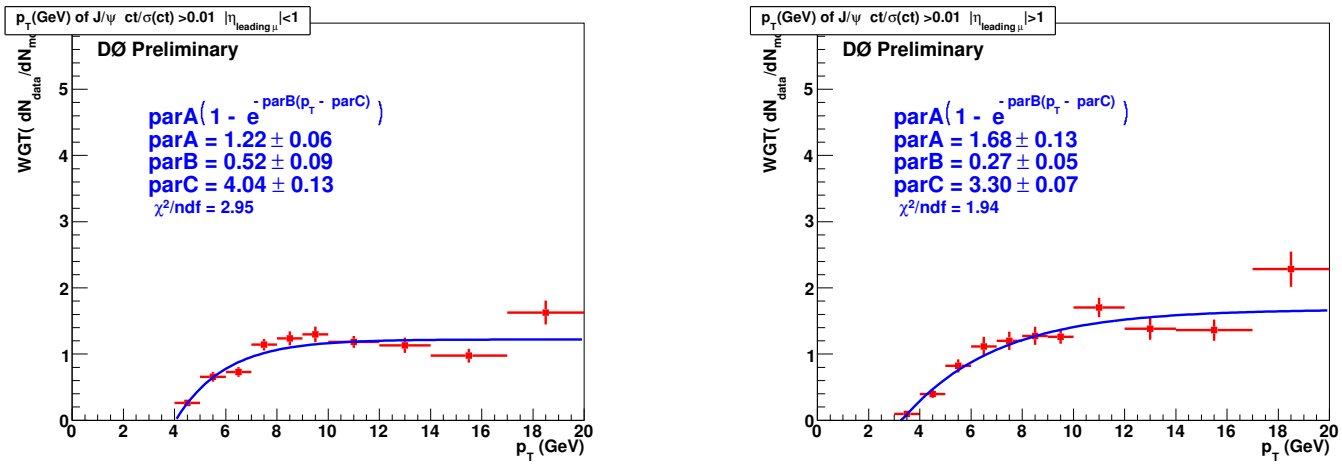

FIG. 10: The ratio of the numbers of J/ψ mesons originating from the decay $B_s^0 \to J/\psi\phi$ in data and Monte Carlo as a function of $p_T(J/\psi)$. Left: central region, Right: forward region.

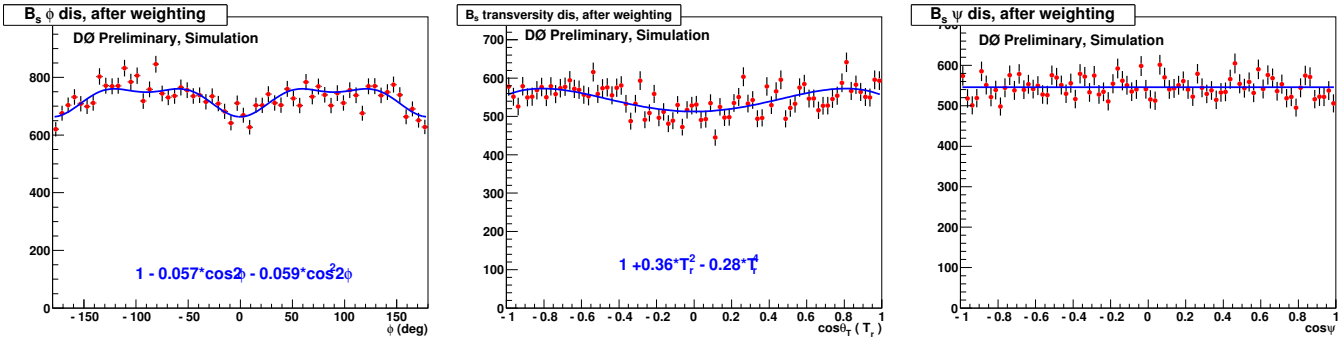

FIG. 11: The D0 detector acceptance as a function of a:transversity azimuthal angle φ, b:transversity polar angle $\cos\theta$, c:$\cos\psi$. It is obtained by weighting the accepted MC events, generated uniformly in the angular space, by the factors shown in Fig. 10.

APPENDIX C: ENSEMBLE STUDY

We have done a study of an ensemble of ≈ 2000 "toy" Monte Carlo experiments, each with similar statistical sensitivity as the data, generated according to the parameter values as obtained in the fit with constrained strong phases. The distributions of generated input quantities for one experiment are compared to data in Fig. 12. They are in good agreement.

Figure 13 shows the distributions of the fitted values of physics parameters: $c\overline{\tau}_s$, $A_\perp(0)$, $\Delta\Gamma_s$. and $\phi_s^{J/\psi\phi}$ distributions of their statistical uncertainties, and pull distributions. There is no significant bias in the fit results, and all statistical uncertainties are within their expected ranges. There is a small absolute bias in $A_\perp(0)$ of -0.01 (1/3 of the statistical uncertainty).

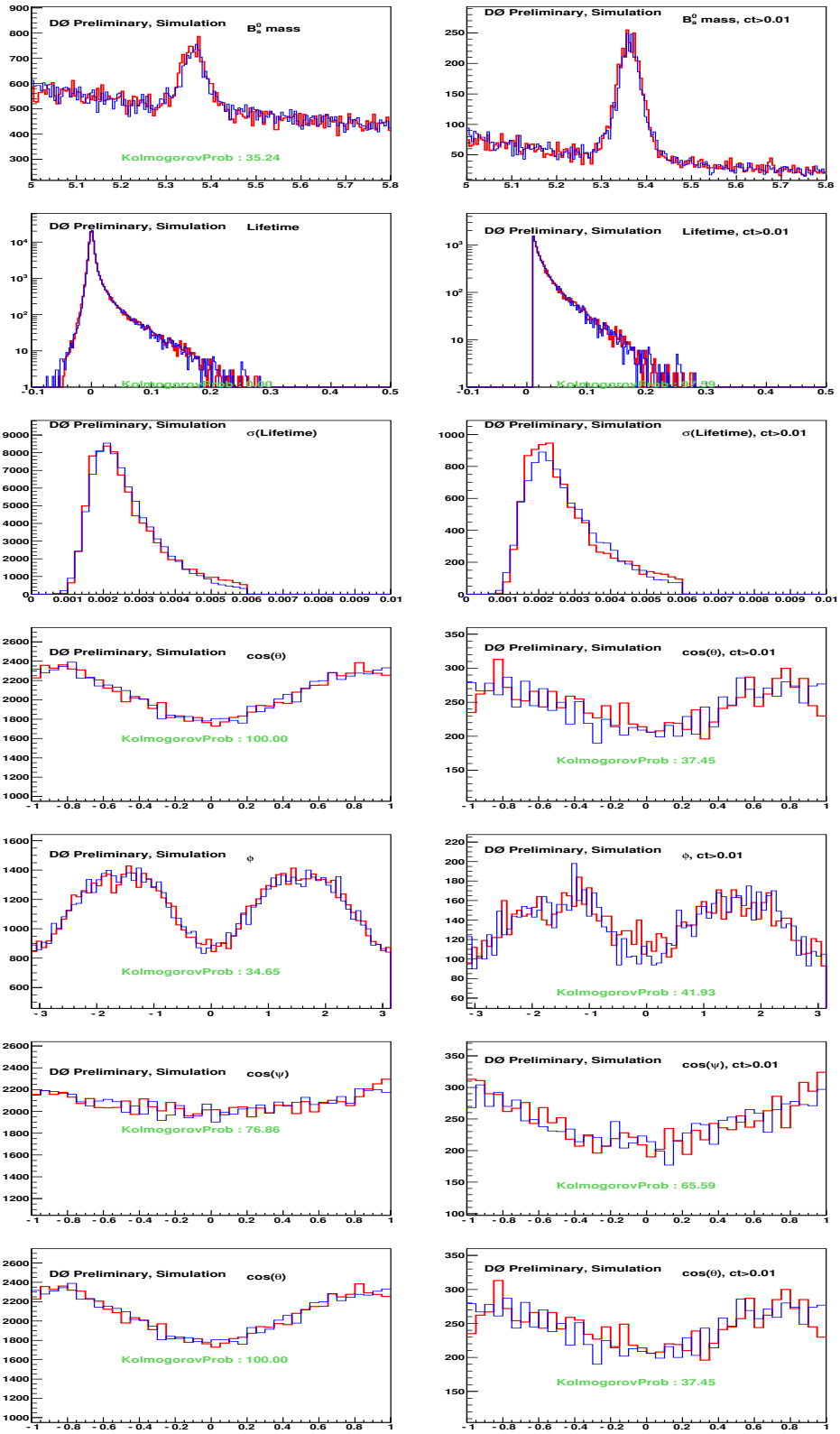

FIG. 12: A comparison of input data in the real experiment and in one generated pseudoexperiment. Left: all events, Right: $ct > 100$ μm.

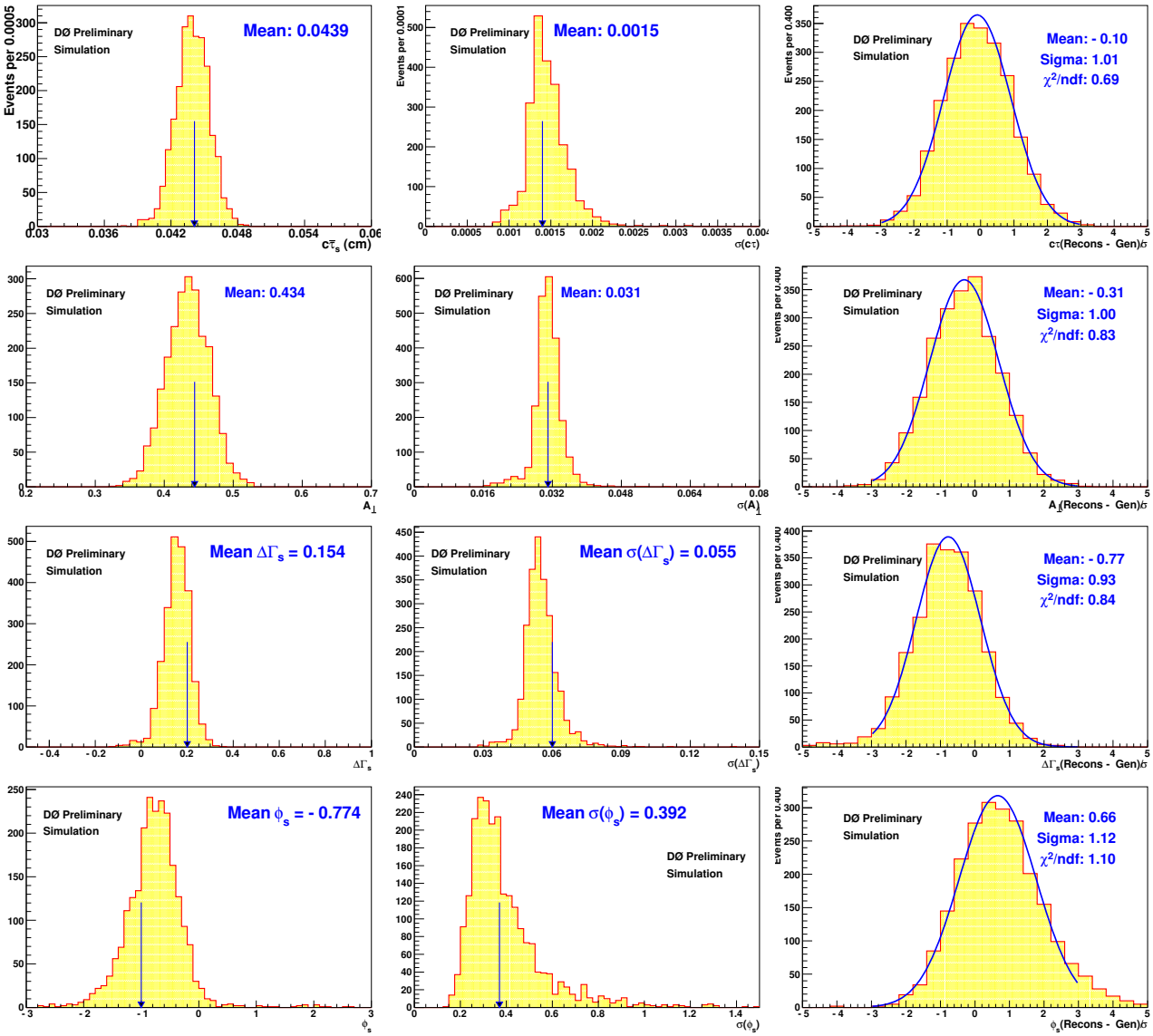

FIG. 13: Results of the ensemble test. The first column shows the distributions of $c\overline{\tau}_s$, $A_\perp(0)$, $\Delta\Gamma_s$, and $\phi_s^{J/\psi\phi}$, returned by fits with constrained strong phases, to pseudo-experiments (see text). The arrows indicate the input values, as given in the first column of Table II. The second column shows the corresponding distributions of parabolic errors. The arrows indicate the values obtained in this analysis. The third column shows the pull distributions.